Published in final edited form as:

Prostate. 2015 October ; 75(14): 1601–1609. doi:10.1002/pros.23036.

Metabolic Response of Prostate Cancer to Nicotinamide Phophoribosyltransferase Inhibition in a Hyperpolarized MR/PET Compatible Bioreactor

Kayvan R. Keshari[1,2,†], **David M. Wilson**[3], **Mark Van Criekinge**[3], **Renuka Sriram**[3], **Bertram L. Koelsch**[3], **Zhen J. Wang**[3], **Henry F. VanBrocklin**[3], **Donna M. Peehl**[4], **Tom O'Brien**[5], **Deepak Sampath**[5], **Richard A. D. Carano**[6], and **John Kurhanewicz**[3]

[1]Department of Radiology, Memorial Sloan-Kettering Cancer Center (MSKCC), New York, NY 10065, USA

[2]Molecular Pharmacology and Chemistry Program, Memorial Sloan-Kettering Cancer Center (MSKCC), New York, NY 10065, USA

[3]Department of Radiology and Biomedical Imaging, University of California, San Francisco, San Francisco, CA 94158, USA

[4]Department of Urology, Stanford University, Stanford, CA 94305, USA

[5]Department of Translational Oncology, Genentech, Inc., South San Francisco, CA, 94080, USA

[6]Department of Biomedical Imaging, Genentech, Inc., South San Francisco, CA, 94080, USA

Abstract

Background—Metabolic shifts in disease are of great interest for the development of novel therapeutics. In cancer treatment, these therapies exploit the metabolic phenotype associated with oncogenesis and cancer progression. One recent strategy involves the depletion of the cofactors needed to maintain the high rate of glycolysis seen with the Warburg effect. Specifically, blocking nicotinamide adenine dinucleotide (NAD) biosynthesis via nicotinamide phosphoribosyltransferase (NAMPT) inhibition depletes cancer cells of the NAD needed for glycolysis. To characterize this metabolic phenotype *in vivo* and describe changes in flux with treatment, non-invasive biomarkers are necessary. One such biomarker is hyperpolarized (HP) [1-^{13}C] pyruvate, a clinically translatable probe that allows real-time assessment of metabolism.

Methods—We therefore developed a cell perfusion system compatible with HP magnetic resonance (MR) and positron emission tomography (PET) to develop translatable biomarkers of response to NAMPT inhibition in reduced volume cell cultures.

Results—Using this platform, we observed a reduction in pyruvate flux through lactate dehydrogenase with NAMPT inhibition in prostate cancer cells, and showed that both HP lactate and 2-[^{18}F] fluoro-2-deoxy-D-glucose (FDG) can be used as biomarkers for treatment response of

[†]Correspondence and Reprint Request: Kayvan R. Keshari, Ph.D., Assistant Member, Department of Radiology and Molecular Pharmacology and Chemistry Program, Memorial Sloan Kettering Cancer Center, 1275 York Avenue, New York, NY 10065, Phone: (646) 888-3631, Fax: (646) 422-0247, rahimikk@mskcc.org.

such targeted agents. Moreover, we observed dynamic flux changes whereby HP pyruvate was re-routed to alanine, providing both positive and negative indicators of treatment response.

Conclusions—This study demonstrated the feasibility of a MR/PET compatible bioreactor approach to efficiently explore cell and tissue metabolism, the understanding of which is critical for developing clinically translatable biomarkers of disease states and responses to therapeutics.

Keywords

translational biomarkers; metabolism; metabolic flux; NAMPT; MRS

INTRODUCTION

There is mounting evidence that changes in the metabolism of a biological system are associated with progression to a given disease state (1) (2,3). Aberrations in the metabolism of substrates, such as glucose and glutamine, have been linked to not only cancer (4,5), but also a wide range of other diseases(6) and changes in microenvironments (7,8). Thus, there has been a renewed interest in the field of metabolism, both at steady state and in dynamic flux, and its effect on tumor growth and response to therapy. Small changes in the tumor microenvironment, such as pH, oxygenation and substrate concentrations can lead to instantaneous changes in metabolism. With this in mind, metabolism has been pursued for the development of both therapeutics and clinically relevant biomarkers for disease and response to therapy.

One recent therapeutic target is nicotinamide phosphoribosyltransferase (NAMPT), an enzyme needed for NAD biosynthesis. NAD has been shown to play an essential role in cellular metabolism, most importantly as a cofactor for the redox reactions of glycolysis including ATP production. Biosynthesis of NAD in mammalian tumor cells occurs predominantly via a salvage pathway, with phosphorylation of nicotinamide by NAMPT representing the rate-limiting step of NAD biosynthesis(9,10). NAMPT is a dimeric type II phosphoribosyltransferase whose physical structure, both in the presence and absence of small-molecule inhibitors has recently been elucidated (11–13). Cancers that exhibit the Warburg phenotype, namely increased aerobic glycolytic flux and decreased oxidative phosphorylation, demonstrate an increased rate of NAD^+ turnover to meet ATP demand. Additionally, NAD-consuming enzymes such as poly-ADP-ribose polymerases (PARPs) have high activities in rapidly proliferating cells, necessitating a high demand for NAD. Inhibition of NAD biosynthesis thus represents an attractive treatment option. Several small-molecule NAMPT inhibitors have been reported in the literature, including 3-aminopyridine-derived amides that are close relatives of nicotinamide(14). The biosynthesis of NAD including the action of NAMPT inhibitors are summarized in Figure 1b, with two of these agents progressing to clinical trials (GMX-1778 and APO-866)(15–17).

Increasingly, the therapeutic efficacy of anticancer drugs may be monitored by non-invasive molecular imaging technologies, including hyperpolarized ^{13}C magnetic resonance (HP MR) and positron emission tomography (PET). In the case of NAMPT inhibition, an intracellular metabolic imaging strategy is necessary to determine the efficacy of treatment. The recently developed inhibitor GNE-617 (Figure 1) derives from a highly potent amide-

containing class of NAMPT inhibitors with great promise as anti-metabolite agents(11). With this in mind, a cellular system was designed to further interrogate the metabolic effects of GNE-617, to potentially characterize additional non-invasive imaging biomarkers. Ideally, this system would (1) ensure cell viability in a near-physiologic environment and (2) integrate with both NMR and PET for identification of clinically translatable molecular imaging probes. In this work, NAD cofactor depletion using GNE-617 is detected by observing diminished ^{13}C pyruvate to lactate conversion, a NADH-dependent reduction catalyzed by lactate dehydrogenase (LDH).

Cellular perfusion systems, deemed *bioreactors*, provide an environment where cells and tissues can grow or change with control of the environment and intervention (18–22). Bioreactors geared toward metabolic investigation have typically been used on the bench top in conjunction with methods to measure distributions of metabolites and tracers, most of which are destructive. Commonly used analytical techniques such as high-performance liquid chromatography (HPLC), NMR and mass spectroscopy are usually performed on cell extracts (23–25). Several less invasive methods have been used to study the chemistry and biochemistry of perfused cellular systems, but these have significant limitations. Optical methods have been used to characterize living cells, but are not broadly translatable to clinical imaging(26). MRS at thermodynamic equilibrium has also been employed, but is generally limited to the study of a few metabolites at steady state (5,27–29).

Recently, bioreactor platforms have been interfaced with dynamic nuclear polarization (DNP) to study metabolite fluxes at high SNR. Over the last decade, advances in DNP technology(30) have led to dramatic signal enhancement of low γ nuclei, such as ^{13}C and ^{15}N (22,31,32). DNP polarized substrates can be injected into living systems and used to study real-time metabolic conversion, thus representing a new direction in the development of clinically translatable biomarkers (33–38). Hyperpolarized MR studies in traditional 10mm or larger MR-compatible culture systems suffer from the need for cell densities on the order of 10^8 cells(22), impractical for the study of primary cells and tissue cultures. The adaptation of the technology to smaller cultures (5×10^6 cells) is non-trivial and requires the optimization of both engineering parameters (flow rate, MR-compatible mechanical structure) and biochemical variables (dissolved oxygen, real time concentration of glucose). The engineering of more compact systems allows study of primary cultures of cells and tissues, which may be more clinically relevant than other disease models. Such a system could also be extended to interface with other non-invasive techniques for metabolic investigation. As HP ^{13}C MRI moves into the clinic, these systems will facilitate probe discovery and provide the mechanistic insights needed to render *in vivo* data useful.

In this study, we developed a 5mm MR-compatible bioreactor platform that can be interfaced with HP ^{13}C MR and PET for metabolic investigation in small cultures of cells and tissues. This system was used to characterize metabolic re-routing following GNE-617 treatment in human prostate cancer cells.

MATERIALS AND METHODS

MR/PET compatible Bioreactor

Prostate cancer cells (PC-3) were cultured in T150 cm^2 flasks with DMEM medium (supplemented with 10% FBS and Penicillin/Streptomycin) (39). Treated cells were incubated with DMEM media containing 50 μM GNE-617. For bioreactor studies, 10 million PC-3 cells were suspended in 2% alginate and cross-linked in a 150mM $CaCl_2$ solution for encapsulation (22). Cells were cultured in a custom-designed 5mm MR-compatible bioreactor system. The system utilized a completely enclosed perfusion system, providing a continuous flow of 37°C medium (analogous to the culture medium) dynamically oxygenated with 95% Air/5% CO_2. The volumetric flow rate (Q) was 0.5mL/min for all bioreactor studies. Oxygen measurements were made by interfacing a temperature calibrated fiber optic based O_2 sensor (Ocean Optics) before and after the bioreactor chamber. Sensors were placed inside of temperature-controlled chambers to maintain stable measurements. These sensors were used to determine the oxygenation level the exchanger achieved.

NMR Studies

All NMR data were acquired on a narrow-bore 14.1T Varian INOVA (150MHz ^{13}C) equipped with a 5mm broadband probe. Cell viability was assessed acquiring ^{31}P spectra (242MHz ^{31}P) with a 90° pulse and acquire sequence (nt=1024, at=1s, T_R=3s) to assess βNTP resonance. [1-^{13}C]pyruvate was hyperpolarized using the Hypersense™ (Oxford Instruments) as previously described (22). 0.5 mL of 7 mM pyruvate were injected over 30 seconds into the bioreactor where ^{13}C NMR spectra were acquired in intervals of 3 secs using 10° pulses for 300 secs. Peak integrals were calculated for each resonance and fluxes were calculated for label conversion to HP lactate.

microPET Studies

A small animal microPET/CT scanner (Inveon, Siemens Medical Solutions, USA) was used for PET imaging. Medium containing 5 μCi/mL of ^{18}F FDG was perfused through the bioreactor system for 40 min and washed out for 40 min. For the purposes of higher throughput, 4 bioreactors were run concurrently in the PET detector, one containing empty alginate encapsulates as a control. Post-washout, the reactor region was defined as a region of interest and activity was calculated relative to control.

Histopathology

After perfusion in the 5mm bioreactor, encapsulated cells were fixed in formalin and sectioned. In addition to a standard hematoxylin & eosin stain, a dual-stain for KI-67 (proliferation) and Caspase-3 (apoptosis) was performed using a prediluted multiplex cocktail (Biocare Medical).

mRNA expression

Total RNA was isolated from frozen PC-3 cells (n=6) using the TriPure Isolation Reagent (Roche) and reverse transcribed using Superscript III Reverse Transcriptase (Invitrogen)

according to the manufacturer's instructions. PCR primers were obtained from Applied Biosciences (Life Technologies, CA, USA), and real-time PCR determination of cDNA amounts was performed. Relative expression to control gene Cyclophilin was determined using the ΔCt method. Primers were used for monocarboxylate transporters 1 and 4 (MCT1,4), lactate dehydrogenase A and B (LDHA and B) as well as glucose like transporter 1 (GLUT1) and hexokinase 2 (HK2).

Lactate Dehydrogenase Activity

Lactate dehydrogenase (LDH) activity was measured spectrophotometrically by quantifying the linear decrease in NADH absorbance at varying pyruvate (sodium salt) concentrations at 339 nm for 10 minutes. Semi-confluent cells were harvested and 10 million cells were lysed (in buffer with 50 mM Tris pH 8.2, 2 mM DTT, 2 mM EDTA, 1% Triton x-100). LDH assays were then carried out using standard methods. LDH activity was plotted against the pyruvate concentration to arrive at the maximum velocity (V_{max}) and the Michaelis-Menten constant (K_m) using the Lineweaver- Burke plot. Total protein measurement was carried out by the calorimetric Bradford reagent method (Quick Start Bradford Protein Assay from BioRad Laboratories, Hercules, CA, USA).

Data Analysis and Statistics

All NMR data was processed using a combination of ACD Lab 1D and 2D NMR processor (version 9; ACD/Labs, Toronto, Canada). Peak areas or volumes were integrated and used to derive the necessary concentrations. All statistics were calculated using JMP software (SAS Corporation, Cary, NC). All PET data was processed using open source AMIDE software. Significance was reported using a two-sided Student's t-test for all comparisons and a p-value<0.05.

RESULTS AND DISCUSSION

5mm MR-compatible bioreactor design allows increased sensitivity for studying low volume cell cultures

In designing an appropriate system to support living cultures within a high-resolution NMR, a number of design constraints are present. These constraints include both adequate perfusion of cells, and appropriate geometry to yield useable data. Although numerous perfused cellular systems have been described, these are difficult to miniaturize and to use robustly for metabolic studies with injectable agents. We therefore designed a perfusion system to not only provide a constant supply of nutrients and remove waste but also to minimize the perfusion volume and to adapt the apparatus for the NMR. A 3 concentric tube exchanger was designed to create the appropriate cell medium temperature and gas equilibration before the fluid enters the bioreactor (Figure 2). The exchanger overall diameter was configured such that it was compatible with a standard NMR bore diameter (ID 50mm). On one side of the exchanger, manifolds were designed to interface this exchanger with both a peristaltic pump (to deliver cell medium) and water bath pump (to control the heat exchange). On the opposite side, the exchanger was designed for minimal volume connection to the top of the bioreactor construct. Additionally a custom cap was designed for medium delivery and recirculation from the bioreactor through the exchanger.

Two bioreactor constructs were developed one for perfusion of suspended encapsulates where a fret was implemented with 300 μm diameter perfusion holes and a second spindle design for the perfusion of living primary tissues. Recirculation was achieved *via* return fluorinated ethylene propylene (FEP) tubing to the medium reservoir. This configuration created the optimal condition for both modulation of oxygen concentration in medium as well as temperature.

Of critical importance with high-resolution NMR is the ability to homogenize the B_0 field surrounding the perfused cell/tissue constructs, since this facilitates a higher spectral resolution. Given the reduction in sample volume and distribution of the sample in the Z direction, relative to larger reactor constructs (e.g. ≥10mm), a line-width of less than 1Hz in ^{1}H (at 500 MHz) was achieved for bioreactors containing perfusion medium using the constructs for both cell-encapsulate and tissue spindle, and a standard 24 element B_0 shim set. This was achievable due to the material utilized in the construct having a similar magnetic susceptibility to that of water. When cell encapsulates or tissue were introduced into the system, an average line-width of 10.9 ± 0.4 Hz was achieved (Supp Figure 1). The combination of a high mass sensitivity (filling factor) with ideal B_0 field homogeneity under perfusion conditions was critical for the acquisition of multinuclear NMR data from small living cell cultures.

Cell viability and steady-state bioenergetics of encapsulated PC-3 cells in the MR-compatible bioreactor

To establish the viability of cells under continuous perfusion within the 5mm bioreactor design, electrostatically encapsulated PC-3 cells in alginate microspheres(22) were perfused for up to 24 hours. At multiple time points, encapsulates were histopathologically assayed for cell integrity (hematoxylin and eosin, H&E), changes in proliferation (Ki-67) and apoptosis (Caspase-3). Representative histologic sections demonstrated the preservation of cell architecture and viability over time (Supp Figure 2). Encapsulated PC-3 cells continued to proliferate at an analogous rate within the bioreactor as in 2D culture (24 hr) with no significant change in apoptosis as demonstrated by lack of Caspase-3 staining. These data support the preservation of cell homeostasis and growth within the bioreactor construct utilizing the flow conditions described in the Methods.

Encapsulated cells were then perfused within the 5mm MR-compatible bioreactor inside of a standard high-resolution NMR. Acquired ^{31}P NMR spectra (Figure 3B) demonstrate both the high SNR data as well as the ability to resolve and quantify resonances of interest, including the nucleotide triphosphates (NTPs, predominantly ATP), the phosphomonoesters (PC – phosphocholine, PE – phosphoethanolamine) and phosphodiesters (GPC – glycerophosphocholine, GPE – glycerophosphoethanolmaine). These resonances were quantified using an electronic reference standard (ERETIC) (40) and scaled directly to encapsulated cell density (Figure 3C). The concentrations of these metabolites not significantly different from those observed in prior PC3 studies, but were demonstrated using nearly an order of magnitude fewer cells (39).

Hyperpolarized ^{13}C pyruvate metabolism to lactate and ^{18}F FDG accumulation correlate with cell density in PC-3 cells

Given that the 5mm MR-compatible bioreactor provided robust 3D cell cultures, we then interfaced a small volume injection port for the rapid introduction of hyperpolarized (HP) substrates. HP pyruvate was injected into varying densities of PC-3 cells and high conversion to HP Lactate was observed in real time (Figure 3D), enzymatically facilitated by lactate dehydrogenase (LDH, EC 1.1.1.27). High SNR data (average max pyruvate SNR 433 ± 30) was easily obtained, using a 10° pulse, within seconds of the introduced HP Pyruvate and lasted nearly 2 min, allowing for the capture of dynamics. The area under the curve of lactate, relative to the total carbon, was consistently less than 10% (0.068 ± 0.011) implying biochemical kinetics are in the first order regime. Normalizing to cell density, the generation of HP Lactate was proportional to the cell density and demonstrated a significant linear correlation (R^2=0.942). The observed HP lactate was significantly higher than that reported for living human malignant prostate tissue slices in a much larger bioreactor (39), but on the order of those observed in immortal cell cultures (22,31,41).

While this bioreactor was designed for perfusion inside of a standard NMR spectrometer, the extension of its use to other imaging modalities was readily achievable. In order to compare metabolism of HP Pyruvate to glucose uptake in cells, the 5mm MR-compatible bioreactor was placed inside of the detector of a microPET and injected with 2-deoxy-2-[^{18}F] fluoroglucose (FDG). First, FDG was injected into both an empty bioreactor and a bioreactor filled with empty alginate encapsulates to assess delivery kinetics in the system(Supp Figure 3). Empty alginate encapsulates demonstrated a similar release of FDG to free flowing medium, with both regions completely devoid of FDG signal 25 min after initiating the washout. This confirmed that the alginate encapsulates do not trap FDG.

In cell experiments, the encapsulated PC-3 cells in the bioreactor were perfused for 40 minutes in medium containing 5μCi/mL of FDG, and then washed out with FDG free medium. Figure 4 demonstrates the simultaneous imaging of 4 bioreactors with increasing densities of PC-3 encapsulated cells. After 40 minutes of washout, the difference in trapping of ^{18}F is readily observed and is linearly correlated to cell density (R^2=0.98, Figure 4B).

NAMPT inhibition results in marked decrease in HP ^{13}C lactate production and ^{18}F-FDG accumulation in PC-3 cells

One of the major strengths of this approach is the ability to evaluate response to therapy using multi-modality noninvasive and synergistic agents. This response is evaluated in a tightly controlled environment, obviating the need for complicated (and often less relevant) animal models, and using MR and PET probes that are directly translatable to humans. While FDG provides the ability to assess changes in upstream metabolism by targeting glucose uptake through glucose like transporters (predominantly GLUT1) and phosphorylation by hexokinase, HP Pyruvate can access downstream glycolysis at the level of conversion to lactate. Combining these probes can provide a better understanding of whether or not a drug hits its target and is effective.

When PC-3 cells were incubated with NAMPT inhibitor GNE-617, a marked decrease in conversion of HP pyruvate to lactate was observed over time (Figure 5). This corresponded to a simultaneous decrease in ^{18}F-FDG accumulation. These changes were similar to the % change in NAD determined spectophotometrically in PC3 cells following GNE-617 treatment (Supp Figure 4). Decreased uptake of ^{18}F-FDG is likely due to the inhibition of glycolysis, since NAD is required in downstream intermediate biochemical reactions. This decreased glycolytic flux may reflect product inhibition of hexokinase (by accumulated glucose-6-phoshpate) or lowered GLUT transporter expression and recruitment. During this same period of time, ^{31}P bioenergetics, in the form of ATP levels, were not significantly different, implying preservation of cell viability (control relative to 6, 24 and 48 hr time points $P>0.2$ for all time points). This result implies that the decreased HP ^{13}C pyruvate to lactate conversion, and reduced ^{18}F-FDG uptake seen with NAMPT inhibition precede cell death.

ATP levels were also measured *ex vivo* demonstrating no significant change within 48 hours of treatment (Supp Table 1). mRNA expression of relevant monocarboxylate transporters (MCT1 and MCT4), which transport pyruvate and lactate across the cell membrane, as well as lactate dehydrogenase (ldha and ldhb) did not change significantly, as expected (Figure 5C). Additionally, the enzyme activity of LDH did not significantly change with 48 hours of treatment (Supp Table 1). These experiments suggest that the decrease in HP lactate production and decreased accumulation of FDG in GNE-617 cannot be attributed to a change in other related enzymes or transporters and are likely due to the depletion of NAD required for LDH. In fact, at only 6hr post treatment a significant decrease in HP lactate ($p=0.044$) was observed. Additionally, with treatment, an analogous increase in HP alanine was seen. This indicates intracellular availability of HP pyruvate as a substrate, allowing alanine aminotransferase (ALT, EC 2.6.1.12) to dynamically compete with LDH. Therefore, HP pyruvate provides biomarkers for both a negative and positive response to drug targeting by NAMPT inhibition, and such a response is quantitatively demonstrated using this approach.

Decreased uptake of FDG in PC-3 cells following treatment with GNE-617 was not significant at 6 hours but was significant at 24 hours. No significant changes in the expression of the predominant FDG transporter and phosphorylating enzyme (glut1 and hk2, respectively) were observed. Therefore, the temporal changes in HP Lactate generation and FDG uptake are likely linked to the loss of NAD, accumulation of upstream glycolytic intermediates, and subsequent inhibition of glycolysis.

CONCLUSIONS

This study demonstrated the feasibility of using a novel 5mm MR/PET compatible bioreactor approach to robustly explore both cell and primary tissue metabolism at dramatically reduced cell and perfusate volumes. This is critical for studying small quantities of cells and tissues, for example stem cells, primary cell and tissue cultures. Here we applied this new bioreactor platform for metabolic investigation of immortal prostate cancer cells. A multimodality approach combining FDG PET and HP pyruvate MR demonstrated changes in prostate cancer metabolism with response to NAMPT inhibition, a

novel cancer therapy. Ongoing studies are focused on the application of this approach to the characterization of cancer aggressiveness in primary tissue cultures using novel combinations of probes. These studies are needed both to understand response to pharmacologic treatment, and validate the use of HP MR and PET molecular imaging in the clinic.

Acknowledgments

Grant Sponsor: NIH K99/R00 EB014328, R21 CA 17176602, R01 CA166766

References

1. Ward PS, Thompson CB. Metabolic reprogramming: a cancer hallmark even warburg did not anticipate. Cancer Cell. 2012; 21(3):297–308. [PubMed: 22439925]
2. Vander Heiden MG, Cantley LC, Thompson CB. Understanding the Warburg effect: the metabolic requirements of cell proliferation. Science. 2009; 324(5930):1029–1033. [PubMed: 19460998]
3. DeBerardinis RJ, Thompson CB. Cellular metabolism and disease: what do metabolic outliers teach us? Cell. 2012; 148(6):1132–1144. [PubMed: 22424225]
4. Warburg O. On the origin of cancer cells. Science. 1956; 123(3191):309–314. [PubMed: 13298683]
5. DeBerardinis RJ, Mancuso A, Daikhin E, Nissim I, Yudkoff M, Wehrli S, Thompson CB. Beyond aerobic glycolysis: transformed cells can engage in glutamine metabolism that exceeds the requirement for protein and nucleotide synthesis. Proc Natl Acad Sci U S A. 2007; 104(49):19345–19350. [PubMed: 18032601]
6. Rowe I, Chiaravalli M, Mannella V, Ulisse V, Quilici G, Pema M, Song XW, Xu H, Mari S, Qian F, Pei Y, Musco G, Boletta A. Defective glucose metabolism in polycystic kidney disease identifies a new therapeutic strategy. Nat Med. 2013; 19(4):488–493. [PubMed: 23524344]
7. Estrella V, Chen T, Lloyd M, Wojtkowiak J, Cornnell HH, Ibrahim-Hashim A, Bailey K, Balagurunathan Y, Rothberg JM, Sloane BF, Johnson J, Gatenby RA, Gillies RJ. Acidity generated by the tumor microenvironment drives local invasion. Cancer Res. 2013; 73(5):1524–1535. [PubMed: 23288510]
8. Gatenby RA, Gillies RJ. A microenvironmental model of carcinogenesis. Nature reviews Cancer. 2008; 8(1):56–61. [PubMed: 18059462]
9. Revollo JR, Grimm AA, Imai S. The NAD biosynthesis pathway mediated by nicotinamide phosphoribosyltransferase regulates Sir2 activity in mammalian cells. The Journal of biological chemistry. 2004; 279(49):50754–50763. [PubMed: 15381699]
10. Rongvaux A, Galli M, Denanglaire S, Van Gool F, Dreze PL, Szpirer C, Bureau F, Andris F, Leo O. Nicotinamide phosphoribosyl transferase/pre-B cell colony-enhancing factor/visfatin is required for lymphocyte development and cellular resistance to genotoxic stress. J Immunol. 2008; 181(7):4685–4695. [PubMed: 18802071]
11. Zheng X, Bauer P, Baumeister T, Buckmelter AJ, Caligiuri M, Clodfelter KH, Han B, Ho YC, Kley N, Lin J, Reynolds DJ, Sharma G, Smith CC, Wang Z, Dragovich PS, Gunzner-Toste J, Liederer BM, Ly J, O'Brien T, Oh A, Wang L, Wang W, Xiao Y, Zak M, Zhao G, Yuen PW, Bair KW. Structure-based discovery of novel amide-containing nicotinamide phosphoribosyltransferase (nampt) inhibitors. Journal of medicinal chemistry. 2013; 56(16):6413–6433. [PubMed: 23859118]
12. Kang GB, Bae MH, Kim MK, Im I, Kim YC, Eom SH. Crystal structure of Rattus norvegicus Visfatin/PBEF/Nampt in complex with an FK866-based inhibitor. Molecules and cells. 2009; 27(6):667–671. [PubMed: 19533035]
13. Wang T, Zhang X, Bheda P, Revollo JR, Imai S, Wolberger C. Structure of Nampt/PBEF/visfatin, a mammalian NAD+ biosynthetic enzyme. Nature structural & molecular biology. 2006; 13(7): 661–662.
14. Dragovich PS, Zhao G, Baumeister T, Bravo B, Giannetti AM, Ho YC, Hua R, Li G, Liang X, Ma X, O'Brien T, Oh A, Skelton NJ, Wang C, Wang W, Wang Y, Xiao Y, Yuen PW, Zak M, Zhao Q,

Zheng X. Fragment-based design of 3-aminopyridine-derived amides as potent inhibitors of human nicotinamide phosphoribosyltransferase (NAMPT). Bioorganic & medicinal chemistry letters. 2014; 24(3):954–962. [PubMed: 24433859]

15. Cerna D, Li H, Flaherty S, Takebe N, Coleman CN, Yoo SS. Inhibition of nicotinamide phosphoribosyltransferase (NAMPT) activity by small molecule GMX1778 regulates reactive oxygen species (ROS)-mediated cytotoxicity in a p53- and nicotinic acid phosphoribosyltransferase1 (NAPRT1)-dependent manner. The Journal of biological chemistry. 2012; 287(26):22408–22417. [PubMed: 22570471]
16. Zerp SF, Vens C, Floot B, Verheij M, van Triest B. NAD(+) depletion by APO866 in combination with radiation in a prostate cancer model, results from an in vitro and in vivo study. Radiotherapy and oncology : journal of the European Society for Therapeutic Radiology and Oncology. 2014; 110(2):348–354. [PubMed: 24412016]
17. Nahimana A, Attinger A, Aubry D, Greaney P, Ireson C, Thougaard AV, Tjornelund J, Dawson KM, Dupuis M, Duchosal MA. The NAD biosynthesis inhibitor APO866 has potent antitumor activity against hematologic malignancies. Blood. 2009; 113(14):3276–3286. [PubMed: 19196867]
18. Farghali H, Caraceni P, Rilo HL, Borle AB, Gasbarrini A, Gavaler J, Van Thiel DH. Biochemical and 31P-NMR spectroscopic evaluation of immobilized perfused rat Sertoli cells. J Lab Clin Med. 1996; 128(4):408–416. [PubMed: 8833890]
19. Gillies RJ, Galons JP, McGovern KA, Scherer PG, Lien YH, Job C, Ratcliff R, Chapa F, Cerdan S, Dale BE. Design and application of NMR-compatible bioreactor circuits for extended perfusion of high-density mammalian cell cultures. NMR in biomedicine. 1993; 6(1):95–104. [PubMed: 8457432]
20. Macdonald JM, Grillo M, Schmidlin O, Tajiri DT, James TL. NMR spectroscopy and MRI investigation of a potential bioartificial liver. NMR in biomedicine. 1998; 11(2):55–66. [PubMed: 9608589]
21. Mancuso A, Fernandez EJ, Blanch HW, Clark DS. A nuclear magnetic resonance technique for determining hybridoma cell concentration in hollow fiber bioreactors. Biotechnology (N Y). 1990; 8(12):1282–1285. [PubMed: 1366962]
22. Keshari KR, Kurhanewicz J, Jeffries RE, Wilson DM, Dewar BJ, Van Criekinge M, Zierhut M, Vigneron DB, Macdonald JM. Hyperpolarized (13)C spectroscopy and an NMR-compatible bioreactor system for the investigation of real-time cellular metabolism. Magn Reson Med. 2010; 63(2):322–329. [PubMed: 20099325]
23. Miccheli AT, Miccheli A, Di Clemente R, Valerio M, Coluccia P, Bizzarri M, Conti F. NMR-based metabolic profiling of human hepatoma cells in relation to cell growth by culture media analysis. Biochim Biophys Acta. 2006; 1760(11):1723–1731. [PubMed: 17052856]
24. Burgess SC, Weis B, Jones JG, Smith E, Merritt ME, Margolis D, Dean Sherry A, Malloy CR. Noninvasive evaluation of liver metabolism by 2H and 13C NMR isotopomer analysis of human urine. Anal Biochem. 2003; 312(2):228–234. [PubMed: 12531210]
25. Stephanopoulos, G.; Gill, R. Metabolic Engineering. Heidelberg: Springer Berlin; 2001.
26. Luker GD, Luker KE. Optical imaging: current applications and future directions. Journal of nuclear medicine : official publication, Society of Nuclear Medicine. 2008; 49(1):1–4.
27. Gamcsik MP, Bierbryer RG, Millis KK. Noninvasive monitoring of glutathione turnover in perfused MCF-7 cells. Free Radic Biol Med. 2004; 37(7):961–968. [PubMed: 15336312]
28. Beloueche-Babari M, Jackson LE, Al-Saffar NMS, Eccles SA, Raynaud FI, Workman P, Leach MO, Ronen SM. Identification of magnetic resonance detectable metabolic changes associated with inhibition of phosphoinositide 3-kinase signaling in human breast cancer cells. Molecular cancer therapeutics. 2006; 5(1):187–196. [PubMed: 16432178]
29. Eskey CJ, Koretsky AP, Domach MM, Jain RK. Role of oxygen vs. glucose in energy metabolism in a mammary carcinoma perfused ex vivo: direct measurement by 31P NMR. Proc Natl Acad Sci U S A. 1993; 90(7):2646–2650. [PubMed: 8464871]
30. Ardenkjær-Larsen JH, Fridlund B, Gram A, Hansson G, Hansson L, Lerche MH, Servin R, Thaning M, Golman K. Increase in signal-to-noise ratio of > 10,000 times in liquid-state NMR.

Proceedings of the National Academy of Sciences of the United States of America. 2003; 100(18): 10158–10163. [PubMed: 12930897]

31. Harris T, Eliyahu G, Frydman L, Degani H. Kinetics of hyperpolarized 13C1-pyruvate transport and metabolism in living human breast cancer cells. Proceedings of the National Academy of Sciences of the United States of America. 2009; 106(43):18131–18136. [PubMed: 19826085]
32. Keshari KR, Sriram R, Koelsch BL, Van Criekinge M, Wilson DM, Kurhanewicz J, Wang ZJ. Hyperpolarized 13C-pyruvate magnetic resonance reveals rapid lactate export in metastatic renal cell carcinomas. Cancer Res. 2013; 73(2):529–538. [PubMed: 23204238]
33. Kurhanewicz J, Vigneron DB, Brindle K, Chekmenev EY, Comment A, Cunningham CH, Deberardinis RJ, Green GG, Leach MO, Rajan SS, Rizi RR, Ross BD, Warren WS, Malloy CR. Analysis of cancer metabolism by imaging hyperpolarized nuclei: prospects for translation to clinical research. Neoplasia. 2011; 13(2):81–97. [PubMed: 21403835]
34. Keshari KR, Sai V, Wang ZJ, Vanbrocklin HF, Kurhanewicz J, Wilson DM. Hyperpolarized [1-13C]Dehydroascorbate MR Spectroscopy in a Murine Model of Prostate Cancer: Comparison with 18F-FDG PET. Journal of nuclear medicine : official publication, Society of Nuclear Medicine. 2013
35. Gallagher FA, Kettunen MI, Hu DE, Jensen PR, Zandt RI, Karlsson M, Gisselsson A, Nelson SK, Witney TH, Bohndiek SE, Hansson G, Peitersen T, Lerche MH, Brindle KM. Production of hyperpolarized [1,4-13C2]malate from [1,4-13C2]fumarate is a marker of cell necrosis and treatment response in tumors. Proc Natl Acad Sci U S A. 2009; 106(47):19801–19806. [PubMed: 19903889]
36. Gallagher FA, Kettunen MI, Day SE, Hu DE, Ardenkjaer-Larsen JH, Zandt R, Jensen PR, Karlsson M, Golman K, Lerche MH, Brindle KM. Magnetic resonance imaging of pH in vivo using hyperpolarized 13C-labelled bicarbonate. Nature. 2008; 453(7197):940–943. [PubMed: 18509335]
37. Keshari KR, Wilson DM, Chen AP, Bok R, Larson PE, Hu S, Van Criekinge M, Macdonald JM, Vigneron DB, Kurhanewicz J. Hyperpolarized [2-13C]-fructose: a hemiketal DNP substrate for in vivo metabolic imaging. J Am Chem Soc. 2009; 131(48):17591–17596. [PubMed: 19860409]
38. Wilson DM, Keshari KR, Larson PE, Chen AP, Hu S, Van Criekinge M, Bok R, Nelson SJ, Macdonald JM, Vigneron DB, Kurhanewicz J. Multi-compound polarization by DNP allows simultaneous assessment of multiple enzymatic activities in vivo. J Magn Reson. 2010; 205(1): 141–147. [PubMed: 20478721]
39. Keshari KR, Sriram R, Van Criekinge M, Wilson DM, Wang ZJ, Vigneron DB, Peehl DM, Kurhanewicz J. Metabolic reprogramming and validation of hyperpolarized C lactate as a prostate cancer biomarker using a human prostate tissue slice culture bioreactor. Prostate. 2013
40. Albers MJ, Butler TN, Rahwa I, Bao N, Keshari KR, Swanson MG, Kurhanewicz J. Evaluation of the ERETIC method as an improved quantitative reference for 1H HR-MAS spectroscopy of prostate tissue. Magn Reson Med. 2009; 61(3):525–532. [PubMed: 19235261]
41. Day S, Kettunen M, Gallagher F, Hu D. Detecting tumor response to treatment using hyperpolarized 13C magnetic resonance imaging and spectroscopy. Nature medicine. 2007
42. Hassan SB, Lovborg H, Lindhagen E, Karlsson MO, Larsson R. CHS 828 kill tumour cells by inhibiting the nuclear factor-kappaB translocation but unlikely through down-regulation of proteasome. Anticancer research. 2006; 26(6B):4431–4436. [PubMed: 17201165]
43. Bi TQ, Che XM, Liao XH, Zhang DJ, Long HL, Li HJ, Zhao W. Overexpression of Nampt in gastric cancer and chemopotentiating effects of the Nampt inhibitor FK866 in combination with fluorouracil. Oncology reports. 2011; 26(5):1251–1257. [PubMed: 21743967]

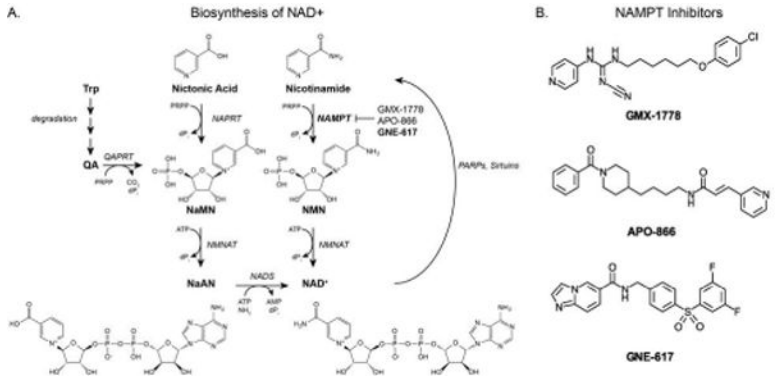

Figure 1.

(A) NAD (nicotinamide adenine dinucleotide) is synthesized *via* a number of pathways. Both Nicotinic acid and Nicotinamide can be converted to NAD. Additionally, when tryptophan (Trp) is degraded, quinolinic acid (QA) is enzymatically converted to nicotinic acid mononucleotide (NaMN) and subsequently nicotinic acid adenine dinucleotide (NaAD) and later NAD. Due to increased activity of PARPs, Sirtuins, etc…NAD+ is consumed with nicotinamide as a product. (B) NAMPT inhibitors. GMX-1776 (CHS-828) is a pyridly cyanoguanidine NAMPT inhibitor that also inhibits the NF-kB pathway(42). APO-866 (Daporinad or FK866) is another NAMPT inhibitor, which also potentially inhibits VEGF(43). GNE-617 is a recently developed amide-containing inhibitor(11).

Abbreviations: NaMN – nicotinic acid mononucleotide, NMN – nicotinamide mononucleotide, NAPRT – nicotinate phosphoribosyltransferase (EC 2.4.2.11), QAPRT – quinolate phosphoribosyltransferase (EC 2.4.2.19), NMNAT – nicotinamide mononucleotide adenylyl-transferase (EC 2.7.7.1), NAMPT – nicotinamide phosphoribosyltransferase (EC 2.4.2.12), NADS – NAD+ synthetase (EC 6.3.1.5), PRPP – 5-phospho-alpha-D-ribose 1-diphosphate dPi – diphosphate

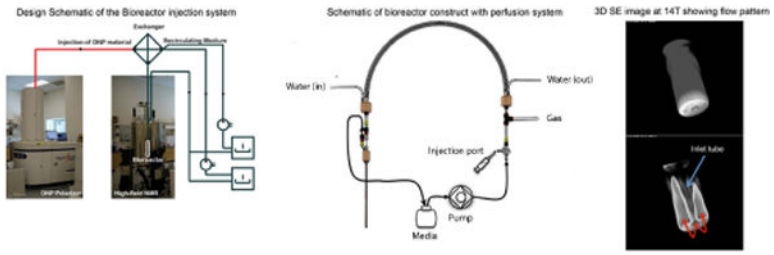

Figure 2.

(Left) Design schematic of bioreactor approach interfaced with hyperpoloarized injection. (Middle) Bioreactor loop construction, including 3 concentric tube exchanger and continuous flow. (Right) 3D ^{1}H T_2-weighted spin-echo image (T_E = 13.897ms, T_R = 1s, FOV 1 × 1 × 1mm, voxel size of 0.0038mm^3) acquired at 14.1T (Wide-bore micro-imaging system, using a 10mm broadband probe, Agilent) of the bioreactor under continuous flow. The flow pattern at the base of the inlet tube is shown and demonstrates the media flow into the bioreactor through an inlet tube in the center and outflow around the exterior of the inlet tube.

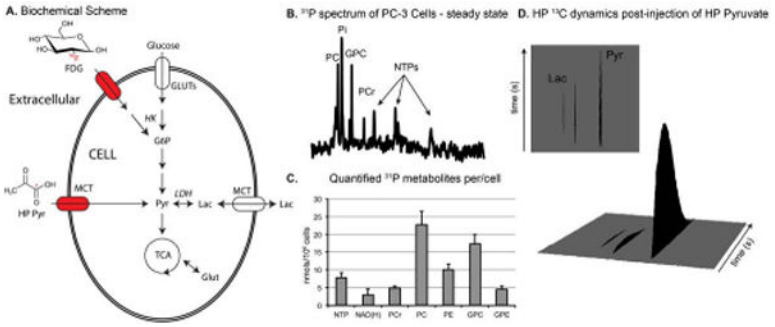

Figure 3.

(A) Biochemical Scheme of cellular metabolism when utilizing hyperpolarized [1-^{13}C] pyruvate (HP Pyr) and ^{18}F-deoxyglucose (FDG). (B) Representative ^{31}P NMR spectra of 15 × 10^6 living PC-3 cells within the 5mm bioreactor. (C) Average concentrations of observed metabolites (n = 6). (D) ^{13}C NMR spectra acquired on PC-3 cells post injection of 7mM HP Pyr. Time resolved data is shown with 3 sec resolution, acquired with a 10°pulse and acquire scheme.

Abbreviations: G6P – glucose-6-phosphate, Pyr – pyruvate, Lac – lactate, Glut – glutamine, GLUTs – glucose transporters, MCT – monocarboxylate transporters, HK – hexokinase (EC 2.7.1.1), LDH – lactate dehydrogenase (EC 1.1.1.27), TCA – tricarboxylic acid cycle, NTPs – nucleoside triphosphates, predominantly ATP, PC – phosphocholine, PE – phosphoethanolamine, GPC – glycerophosphocholine, PCr – phosphocreatine, Pi – inorganic phosphate, GPE – glycerophosphoethanolmaine.

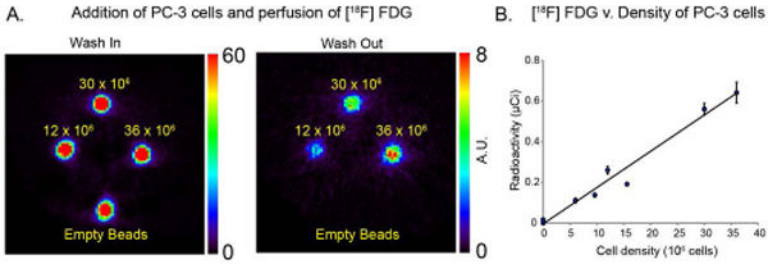

Figure 4.

(A) Imaging of 4 bioreactors simultaneously with a wash-in of FDG of 40 min and analogous wash-out of 40 min. The number of cells in each case is depicted, demonstrating enhanced retention of tracer at higher cell-counts. (B) Plot of accumulated radioactivity after wash-out of the tracer, with a linear correlation (R^2=0.98), as expected for increasing cell density.

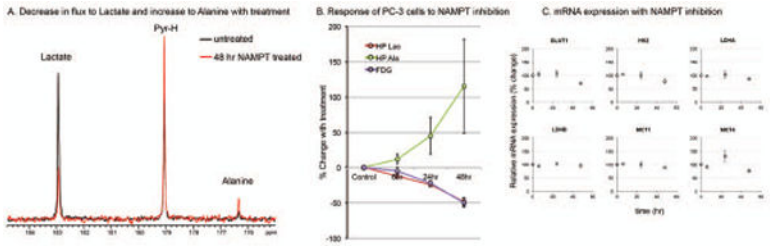

Figure 5.

Demonstration of translatable biomarker response in PC-3 cells by NAMPT inhibition using GNE-617, which prevents the regeneration of NAD. (A) HP ^{13}C NMR spectra demonstrate the marked decrease in HP Lactate with treatment and increase in HP Alanine. (B) Analogous decrease in FDG accumulation, indicative of changes in glycolysis due to NAMPT inhibition. (C) mRNA expression of cells with treatment, suggesting that the biomarker changes observed are due to a decrease in the cofactor NAD and not changes in expression of the relevant transporters and enzymes.